Food & Function

ROYAL SOCIETY OF CHEMISTRY

PAPER

View Article Online
View Journal | View Issue

Cite this: *Food Funct.*, 2025, **16**, 9006

Urolithins and their phase II conjugates cross the blood–brain barrier and exert a stimulus-dependent anti-inflammatory effect on microglial cells by inhibiting NF-κB nuclear translocation

Beatriz Garay-Mayol,[a] Juan Antonio Giménez-Bastida,[a,b] Diego José López-Cánovas,[a] Sabrina Poveda-Lora,[a] Silvia Navarro-Orcajada,[a] María Alexandra Brito,[c] Claudia Nunes dos Santos,[d,e] Juan Carlos Espín,[a,b] María Ángeles Ávila-Gálvez[a,b] and Antonio González-Sarrías *[a]

Neuroinflammation plays a central role in ageing and the progression of neurodegenerative diseases. Epidemiological studies suggest that consuming ellagitannins (ETs)- and ellagic acid (EA)-rich foods like pomegranate or walnuts may confer neuroprotective benefits. However, ETs and EA have low bioavailability and are extensively metabolized by the human gut microbiota into urolithins (Uros), which circulate mainly as glucuronide and sulphate conjugates. This study evaluated the ability of the main colonic Uros (Uro-A, Uro-B, and IsoUro-A), and their respective phase II conjugates, to cross human brain microvascular endothelial cells (HBMECs) as an *in vitro* model of the blood–brain barrier (BBB), and assessed their anti-(neuro)inflammatory effects on the BBB endothelium and human microglial cells (HMC3) under different inflammatory stimuli. UPLC-qTOF-MS analyses revealed that all Uros and their conjugates crossed the BBB, with Uro-B and its sulphate showing the highest transport efficiency. Moreover, Uros preserved BBB integrity against TNFα-induced damage. In HMC3 cells, all Uros significantly reduced IL-6 secretion, whereas only the free forms decreased IL-8 levels under LPS stimulation. However, no effects were observed in TNFα-stimulated cells, indicating a stimulus-dependent response. Additionally, all Uros prevented NF-κB nuclear translocation in LPS-treated cells, and Uro-A specifically interfered with the canonical MyD88-dependent arm of TLR4 signalling, without broadly inhibiting receptor expression or affecting the TRIF-dependent branch. These findings suggest that consuming ETs and EA-rich foods as precursors of Uros could exert anti-neuroinflammatory activity, potentially preventing or delaying the development of neurodegenerative diseases.

Received 29th August 2025,
Accepted 6th November 2025

DOI: 10.1039/d5fo03678j

rsc.li/food-function

Introduction

Neurodegenerative diseases (ND), such as Alzheimer's and Parkinson's diseases, are among the most important public health problems in developed countries, and their prevalence is constantly rising due to increased life expectancy.[1,2] These diseases involve the progressive loss of neurons in specific regions of the central nervous system (CNS), leading to impaired movement and/or cognitive decline (dementia, thinking and behaviour detriment, among others). Neuroinflammation, driven by activated microglia cells, is among the hallmarks of ND and is intricately linked to the onset and progression of these diseases.[3–5] Intrinsic and extrinsic factors, such as infections or oxidative stress, can induce neuroinflammation and activate specific signalling pathways in microglial cells. Once activated, microglia release pro-inflammatory cytokines such as tumour necrosis factor alpha (TNFα), IL-6, IL-8, and IL-1β, among others, which amplify the inflammatory response and contribute to neuronal damage.[5–8] Since effective treatments against ND remain limited and brain changes can begin many years before symptoms appear, prevention has become a key focus.[9] Consequently, there is a growing interest in identifying natural compounds with anti-(neuro)inflammatory and neuro-

[a]*Research Group on Quality, Safety and Bioactivity of Plant Foods, CEBAS-CSIC, 30100 Campus de Espinardo, Murcia, Spain. E-mail: agsarrias@cebas.csic.es*
[b]*Laboratory of Food & Health, Research Group on Quality, Safety and Bioactivity of Plant Foods, CEBAS-CSIC, 30100 Campus de Espinardo, Murcia, Spain*
[c]*Research Institute for Medicines (iMed.ULisboa), Department of Pharmaceutical Sciences and Medicines, Faculty of Pharmacy, Universidade de Lisboa, Av. Prof. Gama Pinto, 1649-003 Lisbon, Portugal*
[d]*NOVA Medical School Faculdade de Ciências Médicas, NMS/FCM, Universidade Nova de Lisboa, 1169-056 Lisbon, Portugal*
[e]*iNOVA4Health, NOVA Institute Medical Systems Biology, NIMSB, Universidade Nova de Lisboa, 1099-085 Lisboa, Portugal*

protective properties as a non-pharmacological strategy to support long-term brain health. In this context, diet plays a crucial role, as accumulating evidence suggests that dietary interventions, with particular attention given to polyphenol-rich foods, may offer benefits for brain health.[10–13]

Ellagitannins (ETs) and ellagic acid (EA), found abundantly in pomegranates, walnuts, and some berries like strawberries, raspberries, or blackberries, have been associated with beneficial properties on cognitive health.[14,15] However, due to their low bioavailability and extensive metabolism by the gut microbiota, the biological effects of ETs and EA are largely attributed to their gut microbiota-derived metabolites, known as urolithins (Uros).[16,17] In humans, three major final Uros have been identified as products of ETs and EA metabolism, including Uro-A, Uro-B, and IsoUro-A. However, their intestinal biosynthesis depends on the individuals' gut microbial composition and functionality. This gives rise to considerable interindividual variability, leading to the definition of specific urolithin metabotypes (UMs). In this line, three well-established UMs have been described based on the final Uros produced: (i) metabotype A (UM-A), characterised by the exclusive production of Uro-A, (ii) metabotype B (UM-B) that yields Uro-B and IsoUro-A in addition to Uro-A, and (iii) metabotype 0 (UM-0), in which individuals do not produce these final Uros.[17–19] Thus, in contrast to the poor absorption of ETs and EA, Uros can reach relevant concentrations in the bloodstream (in the low micromolar range), primarily circulating as phase II conjugates (glucuronides and sulphates).[17] Therefore, for the last decade, Uros have attracted great interest in combating ND due to their well-demonstrated *in vitro* and *in vivo* anti-inflammatory effects.[15,17] In this line, numerous studies using a wide range of cellular and animal models of ND have demonstrated the neuroprotective and anti-inflammatory effects of Uros, particularly Uro-A, by attenuating pro-inflammatory responses including IL-1β, IL-6, and TNFα in microglial cells and neuronal tissues, but also promoting mitophagy, improving mitochondrial function and antioxidant machinery, *etc*.[15,20–23] However, most of this research has focused on the free forms, while the conjugated metabolites, glucuronides and sulphates, which are the predominant circulating forms and therefore, the capacity of these conjugates to cross the blood–brain barrier (BBB) and exert biological effects in the CNS remains largely unexplored. In this context, to date, one *in vitro* study has shown that phase II conjugation limits the protection against oxidative stress-induced apoptosis in SH-SY5Y neuroblastoma cells, compared to the free forms, *i.e.*, Uro-A, Uro-B, and IsoUro-A.[24] However, whether the phase II conjugation could limit the anti-(neuro)inflammatory effect of Uros is still unexplored. Besides, regarding the ability of Uros to cross the BBB, earlier animal studies detected Uro-A in brain tissues. However, these authors analysed brain samples that were either not perfused or enzymatically treated with glucuronidase and sulfatase following oral or intravenous administration of Uros in rodents.[25–27] These approaches limited the ability to determine whether free, but also conjugated forms, truly reach the brain parenchyma. Furthermore, the presence of Uros in non-perfused brains could reflect residual blood content rather than actual brain penetration. Notably, a recent study has provided the first unequivocal evidence of the presence of Uro-A sulphate and free Uro-A, but not glucuronides, in perfused mouse brains after intraperitoneal administration of free Uro-A, confirming that both free Uro-A and its sulphate conjugate can cross the BBB and reach the brain parenchyma.[28] In addition, more recently, Ávila-Gálvez *et al.* (2025)[29] explored the use of exosomes (EXOs) as nanocarriers to enhance the delivery of Uros to the brain. In agreement with the mouse study,[28] no glucuronide conjugates were detected in the brain regardless of whether Uros were intravenously administered freely or encapsulated in EXOs.[28] In that study, only sulphate of Uro-A and Uro-B were detected when free Uro-A or Uro-B were administered, supporting the previous mouse results, and thus, underscoring the potential of Uros to exert biological effects in the CNS.[29] However, in addition to the limited exploration of the neuroprotective effects of conjugated urolithins, it remains unclear whether their conjugation could restrict their ability to cross the BBB. Therefore, understanding their ability to cross the BBB and distinguishing between free forms and their phase II conjugates' ability to modulate neuroinflammation is essential for accurately assessing their relevance to brain health.

Accordingly, this study aims to compare, for the first time, the ability of the main free Uros (Uro-A, Uro-B, and Iso-UroA) and their circulating phase II conjugates (glucuronides and sulphates) to cross the BBB using an *in vitro* model based on human brain microvascular endothelial cells (HBMECs). We further aim to assess the anti-(neuro)inflammatory effect on the BBB endothelium as well as on human microglial cells (HMC3) stimulated with two different inflammatory insults (LPS and TNFα). Furthermore, this study explored the mechanism of action underlying the neuroprotective effects of these metabolites using immunocytochemistry, *in silico* docking analysis, and molecular biology techniques. Overall, this study provides new insights into the potential direct mechanisms of action of Uros that can reach brain tissue, aiming to determine whether these circulating microbial metabolites may contribute to the neuroprotective effect attributed to the consumption of ETs and EA sources (*e.g.*, pomegranate, walnuts, or berries), which act as Uros precursors, thereby supporting their potential in the prevention or delay of ND.

Materials and methods

Reagents

Urolithin (Uro) metabolites used in this study included the free forms Uro-A, Uro-B, and IsoUro-A, as well as their phase II conjugated derivatives. The conjugates comprised: Uro-A 3-*O*-glucuronide (Uro-A 3-glur), Uro-A 8-*O*-glucuronide (Uro-A 8-glur), Uro-A sulphate (Uro-A sulf), Uro-B glucuronide (Uro-B glur), Uro-B sulphate (Uro-B sulf), IsoUro-A 3-*O*-glucuronide (IsoUro-A 3-glur), and IsoUro-A 9-*O*-glucuronide (IsoUro-A 9-glur). All compounds were chemically synthesized and puri-

fied to >98% purity by Villapharma Research S.L. (Parque Tecnológico de Fuente Álamo, Murcia, Spain). Trypan blue, bovine serum albumin (BSA), MTT (3-(4,5-dimethylthiazol-2-yl)-2,5-diphenyltetrazolium bromide), sodium fluorescein (Na-F), lipopolysaccharide (LPS), tumour necrosis factor-alpha (TNFα), and Triton X-100 were purchased from Sigma-Aldrich (St Louis, MO, USA). HPLC-grade acetonitrile (ACN), formic acid, methanol (MeOH), and dimethyl sulfoxide (DMSO) were obtained from Panreac (Barcelona, Spain). Phosphate buffer saline (PBS) and paraformaldehyde (PFA) 4% were obtained from Fisher Scientific (Madrid, Spain). Ultrapure Millipore water was used throughout the study.

Cell lines and culture conditions

The human microglia cell line (HMC3) was kindly provided by Dr Nunes Dos Santos (NOVA Medical School, Portugal) and was cultured in Dulbecco's modified Eagle's medium (DMEM) enriched with 10% v/v foetal bovine serum (FBS), according to the ATCC recommendations. The growth media also contained 2 mM glutamine and 1% v/v antibiotic solution (100 U mL^{-1} penicillin and 100 μg mL^{-1} streptomycin) (Gibco, Invitrogen S. A., Barcelona, Spain).

A cell line of human brain microvascular endothelial cells (HBMECs), derived from primary cultures of HBMECs transfected with SV40 large T antigen[30] was grown in Roswell Park Memorial Institute (RPMI) medium (Sigma-Aldrich) with the addition of 10% FBS and 10% Nu-Serum IV (BD Biosciences, Madrid, Spain), and supplemented with 2 mM L-glutamine, 1% v/v non-essential amino acids, 1 mM sodium pyruvate and 1% v/v antibiotic solution (Gibco, Invitrogen S.A., Barcelona, Spain).

Both cell lines were incubated at 37 °C in a humidified atmosphere of 95% air/5% CO_2.

In vitro blood–brain barrier transport

The *in vitro* blood–brain barrier (BBB) transport model using HBMECs, following an established protocol.[31,32] Briefly, HBMECs were seeded onto 12-well Transwell® inserts (12 mm diameter, 0.4 μm pore size polyester membrane; Corning, Madrid, Spain), previously coated with rat tail collagen type I (Corning Costar Corp., Arizona, USA). Then, cells were maintained for 6–7 days to allow the formation of confluent monolayers appropriate for modelling the BBB at 37 °C in a humidified incubator with 5% CO_2. Transport assessments were performed using Hanks' Balanced Salt Solution (HBSS), containing 0.1% v/v FBS. Cells on the apical side of the monolayer were exposed to each Uro and their conjugated metabolites (5 μM) for 2 h. To verify the integrity of the endothelial barrier, transendothelial electrical resistance (TEER) was recorded at the beginning (0 h) and end (2 h) incubation time points with each treatment, using an EVOM2 Epithelial Volt Ohm Meter (World Precision Instruments, Inc., USA). Media samples collected from the apical and basolateral compartments were stored at −80 °C until further analysis by UPLC-ESI-qTOF-MS. Endothelial transport of each compound was expressed as a percentage (%) calculated from the concentration in the basolateral compartment relative to the total concentration in both compartments (n = 3). Data are presented as mean ± SD. Different letters indicate statistically significant differences (P < 0.05).

In vitro blood–brain barrier disruption

To mimic an inflammatory environment and BBB disruption, HBMECs were treated with 10 ng mL^{-1} of TNFα in the apical compartment, and incubated for 24 hours to promote endothelial activation and compromise barrier integrity. TNFα was selected as the sole inflammatory stimulus based on preliminary assays, which showed it induced a more consistent and pronounced BBB disruption than LPS, IFN-γ, IL-1β, or their combinations.

Paracellular permeability of the monolayer was evaluated using Na-F (molecular weight: 376 Da) as a low-molecular-weight tracer. After 2 hours of incubation with the fluorescent probe, samples were collected from the basolateral compartment and the fluorescence intensity measured using a microplate reader (FLUOstar Omega, BMG LABTECH, Ortenberg, Germany) (excitation/emission: 460/528 nm). The endothelial permeability coefficient (*Pe*, cm min^{-1}) was calculated based on the rate of Na-F passage across the monolayer, following previously established protocols.[33] Results were expressed as the percentage of variation in *Pe* relative to untreated control cells. Throughout all experiments, barrier integrity was simultaneously monitored by measuring TEER at the beginning and end of the incubation period.

Cytokine analysis in microglia cells

HMC3 cells were seeded at 75 000 cells per well in 24-well plates and incubated for 48 hours. Sub-confluent cells were co-treated with TNFα (50 ng mL^{-1}) or LPS (500 ng mL^{-1}) in combination with 5 μM of each Uro, previously filter-sterilized (0.22 μm), for 24 h. Unstimulated cells (0.5% DMSO, CT) served as negative controls. Next, after treatment, the culture medium was collected and frozen at −80 °C until cytokine analysis. IL-6 and IL-8 levels in the culture supernatants were quantified using commercial ELISA kits (PeproTech, Rocky Hill, NJ, USA), with detection limits of 23 pg mL^{-1} and 8 pg mL^{-1}, respectively. Absorbance was measured using a microplate reader (Infinite M200, Tecan, Grödig, Austria), and cytokine concentrations were determined based on standard curves.

The cell viability was measured using the MTT reduction assay at 24 h, as previously described,[34] to confirm that the treatments with all the samples lacked cytotoxic effects. Values are presented as the mean ± standard deviation (SD) from three independent assays (n = 3).

Assessment of NF-κB nuclear translocation by confocal microscopy

HMC3 cells were seeded at 75 000 cells per well on coverslips placed in 24-well plates and grown for 2 days. Once sub-confluent, cells were treated for 45 min with the Uros and inflammatory stimuli described in the previous sections. This incubation time was selected as the optimal period to detect

nuclear translocation, based on preliminary time-course experiments. After treatments, the cells were washed 3 times with PBS, fixed with 4% v/v paraformaldehyde for 15 min, rewashed, and then maintained in PBS at 4 °C until the immunostaining, which was performed within less than 2 weeks.

For the immunostaining, cells were permeabilized with 0.3% v/v Triton X-100 in PBS for 10 min and then blocked with 3% v/v BSA in PBS for 1 h at room temperature. Next, the coverslips were incubated overnight at 4 °C with NF-κB p65 polyclonal antibody (Cell Signalling, #8242, 1 : 1400) as primary antibody. The secondary antibody Alexa Fluor 594 goat anti-rabbit IgG (Invitrogen, #A-11037, 1 : 500) was then incubated for 1 h at room temperature in the dark.

Nuclei were counterstained with Invitrogen™ ProLong™ Diamond Antifade Mountant with DAPI. Between all incubation steps, cells were washed three times with PBS. Negative controls (without primary antibody incubation) were also performed (data not shown). Images were acquired using a confocal microscope, Leica STELLARIS 8 (Wetzlar, Germany), using a 63× glycerol immersion objective.

For semi-quantitative analysis, four fields per condition were acquired and evaluated. Immunofluorescence images obtained by fluorescence microscopy were examined using Icy (Institute Pasteur and France BioImaging, Paris, France) and ImageJ (National Institutes of Health, Bethesda, MD, USA) software. Nuclear cell fluorescence intensity was quantified using 10 cells per field, applying the ellipse tool from Icy software. The representative images were generated in the ImageJ software.

Western blot

Non-confluent HMC3 cells were treated with DMSO (0.5% v/v) as a control, 500 ng mL^{-1} LPS, and 5 μM Uro-A or Uro-A 3-glur alone or in combination with 500 ng mL^{-1} LPS for 24 h. Cell protein extracts obtained in cold RIPA buffer supplemented with a cocktail of protease and phosphatase inhibitors (Roche, Mannheim, Germany) were kept at −80 °C until further analysis. Protein levels were determined using the DC colorimetric kit (Bio-Rad, Barcelona, Spain).

An equal amount of protein obtained from each treatment was resolved using 10% SDS-PAGE gels and transferred to nitrocellulose membranes, which were incubated with primary antibodies (1 : 500–1 : 2500 dilution) followed by HRP-conjugated anti-rabbit or anti-mouse secondary antibodies (1 : 5000 dilution) (Cell Signalling, MA, USA). The primary antibodies used were MyD88 (Santa Cruz, #sc-136970, 1 : 1000), TRIF (Cell Signalling, #4596, 1 : 1000), and toll-like receptor (TLR)4 (Abcam, #76B357.1, 1 : 500). GAPDH (Cell Signalling, D4C6R; #97166) at a 1 : 2500 dilution was used as a loading control. ImageJ v. 1.54D (NIH, USA) was used for densitometric analysis of the protein bands. The assay was repeated 3 times (n = 3).

UPLC-ESI-qTOF analysis of Uros and conjugated metabolites

Cell media collected from each compartment (apical and basolateral) in the transport assays using HBMECs from each compartment (apical and basolateral) were processed and analysed by an ultraperformance liquid chromatographic system (UPLC) coupled to a quadrupole-time-of-flight (QTOF) mass spectrometer, as described elsewhere.[29] Briefly, equal volumes (200 μL) of culture medium from each compartment and ACN : formic acid (98 : 2, v/v) were mixed, vortexed, and centrifuged at 14 000g for 10 min. The supernatant was evaporated to dryness in a Speedvac concentrator (Savant SPD140 DDA), and the residue re-dissolved in 100 μL MeOH and filtered (0.22 μm) before analysis. The injection volume was 5 μL, and the chromatographic conditions used are described in recent studies.[29,35] Identification and quantification of Uro and their conjugates were achieved using authentic standards according to their accurate mass, molecular formula, and isotopic pattern. All calibration curves were obtained for each authentic standard tested, obtaining good linearity (r^2 > 0.999).

In silico docking analysis

Potential interactions between TLR4 and the tested Uros were investigated through molecular docking simulations using the online drug discovery platform Mcule (Mcule Inc., Palo Alto, CA, USA). This platform integrates cheminformatics tools and curated chemical libraries to enable virtual screening. The InChIKeys of each Uro were retrieved from the PubChem database. The crystal structure of human TLR4 TV3 hybrid-MD-2 tetrameric complex bound to the inhibitor eritoran was obtained from the RCSB Protein Data Bank (PDB ID: 2Z65). The Docking (Vina) tool was used to predict binding affinities, with the binding site defined within the hydrophobic pocket of MD-2, and the corresponding docking poses were exported in Protein Data Bank (PDB) format for further visualization. Docking results, including molecular interactions and visualization of ligand–target binding poses, were analysed and rendered using Biovia Discovery Studio 2025 (Dassault Systèmes, San Diego, CA, USA). Docking scores were used to predict the strength and relevance of the ligand–receptor interactions, with more negative values indicating stronger binding affinities.

Statistical analysis

Normally distributed data presented as the mean ± SD come from at least three independent experiments (n = 3). One-way ANOVA followed by Tukey's *post hoc* test was used for multiple group comparisons (*e.g.*, immunofluorescence analysis). For pairwise comparisons (*e.g.*, western blot quantifications), a two-tailed unpaired Student's t-test was used. The software used for graph preparation and statistical analysis was GraphPad Prism 10.1.1. software (GraphPad Software, San Diego, CA, USA). P < 0.05 was considered to be statistically significant.

Results

Urolithins cross the BBB and protect against BBB insult

We initiated our study by examining the BBB permeation and protective effects against an inflammatory stimulus of free and

conjugated Uros in a simplified BBB *in vitro* model based on a biochamber system, where the upper compartment mimics the blood side, the lower one mimics the brain side, and HBMECs at the interface simulate the BBB endothelium.

The ability of different Uros to cross the BBB was assessed by quantifying each metabolite in both the "blood" (apical side) and "brain" (basolateral side) compartments after 2 h of incubation using UPLC-qTOF-MS (Fig. 1A and B). Among the free forms, Uro-B showed the highest transport efficiency across the BBB (22.3 ± 3.4%), likely due to its lower number of hydroxyl groups, which may enhance lipophilicity and passive diffusion, followed by Uro-A and IsoUro-A, which showed

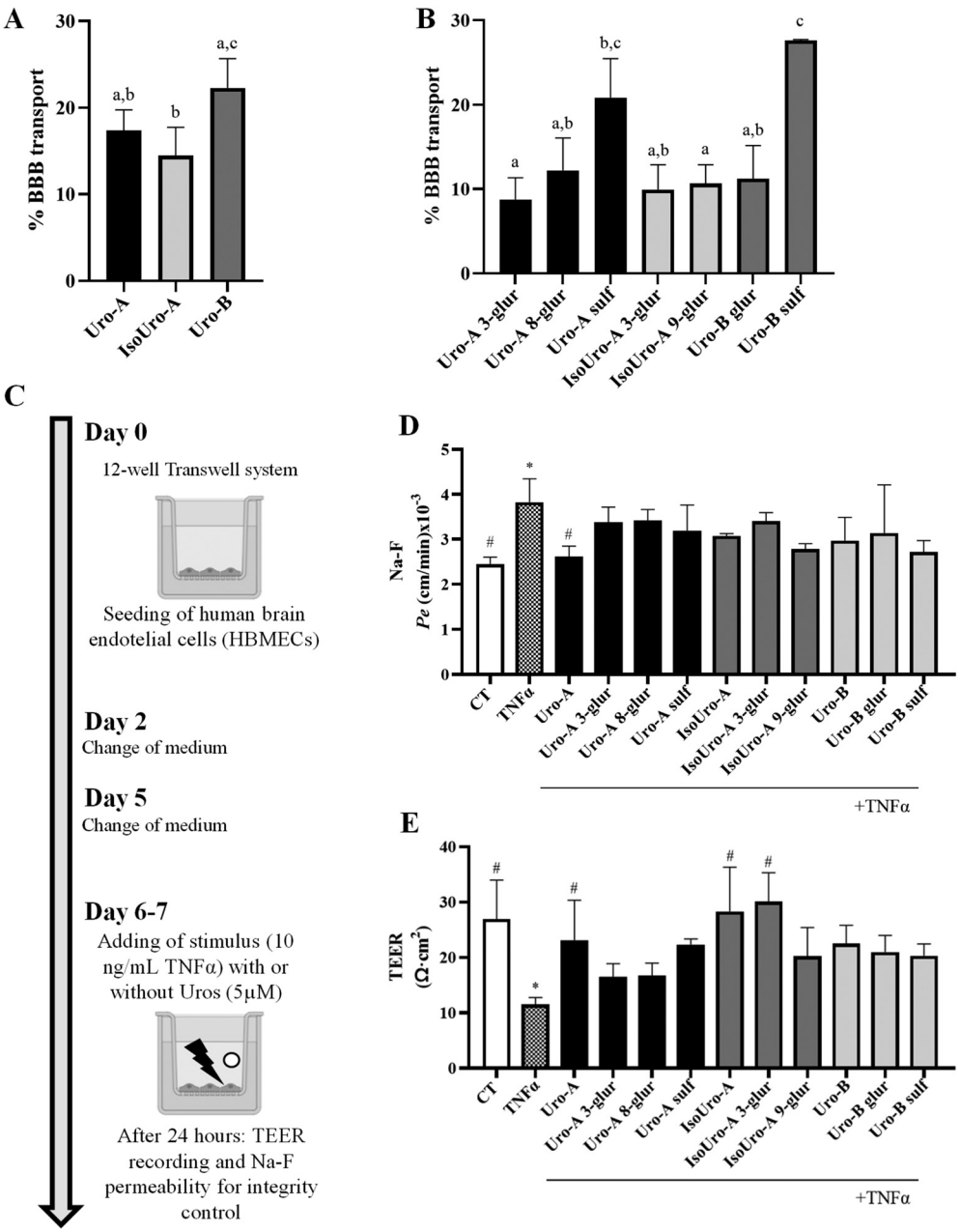

Fig. 1 Effect of urolithins (Uros) on BBB integrity and permeability in an *in vitro* blood–brain barrier (BBB) model. (A) Endothelial transport of the free forms of main Uros at 2 hours of incubation in HBMECs. (B) Endothelial transport of phase II conjugates from the main Uros after 2 hours of incubation in HBMECs. (C) Experimental design used to evaluate the protective effects of all Uros on HBMECs stimulated cells, serving as an *in vitro* model of a disrupted BBB. (D) Mean of apparent permeability coefficient (*Pe*) values for sodium fluorescein (Na-F) at 24 h for vehicle control (CT; vehicle with 0.5% DMSO), TNFα (10 ng mL^{-1}), and Uros-treated cells. (E) Transendothelial electrical resistance (TEER) in HBMECs for CT, TNFα, and Uros at 24 hours. Different lowercase letters indicate statistically significant differences ($P < 0.05$) among the treatments. Statistical differences are denoted as $^{*}P < 0.05$ relative to CT or $^{\#}P < 0.05$ relative to TNFα. All data are presented as means ± SD ($n = 3$). All Uros were tested at a final concentration of 5 μM.

similar transport efficiencies (17.4 ± 2.4% and 14.5 ± 3.3%, respectively) (Fig. 1A). Among the conjugated forms, Uro-B and Uro-A sulfates reached the highest transport efficiency (27.6 ± 0.1% and 20.9 ± 4.6%, respectively), while glucuronides were less efficient.

We next investigated whether Uros could protect the BBB from inflammatory damage. For this purpose, the BBB model was co-treated, alone or in combination with TNFα (10 ng mL^{-1}) and the different Uros (5 μM) for 24 h. The BBB integrity was evaluated using two standard markers of paracellular permeability, *i.e.*, Na-F transport and transendothelial electrical resistance (TEER) (Fig. 1C). Although all Uros and their conjugates tended to reduce the apparent *Pe* for Na-F when compared to TNFα treatment alone, only Uro-A achieved a statistically significant reduction ($P < 0.05$), with *Pe* values approaching those observed in control (non-disrupted) monolayers (Fig. 1D).

TEER measurements confirmed the protective role of several Uros. Uro-A, IsoUro-A, and IsoUro-A 3-glur significantly counteracted the TNFα-induced decrease in TEER, showing statistically significant differences compared to TNFα treatment in the absence of these Uros (Fig. 1E). These findings highlight the potential of specific Uros, both in their free and conjugated forms, to preserve BBB integrity under inflammatory challenge.

Urolithins reduce IL-6 and IL-8 levels in microglia cells, depending on the stimuli

Following the results obtained in the *in vitro* BBB model, we next evaluated the effects of Uros on cytokine release in human microglial cells (HMC3), which represent the resident neuroimmune cells of the brain. For this purpose, two different inflammatory stimuli, which reflect distinct types of inflammatory activation, were used, *i.e.*, lipopolysaccharide (LPS, 500 ng mL^{-1}) and tumour necrosis factor-alpha (TNFα, 50 ng mL^{-1}). LPS mimics bacterial infection, whereas TNFα represents a more physiologically relevant inflammatory signal. Various concentrations were initially tested, and the lowest concentration capable of eliciting a measurable cellular response was selected for subsequent experiments (data not shown).

Under TNFα stimulation, IL-6 and IL-8 levels increased from 435 ± 106 pg mL^{-1} and 295 ± 33 pg mL^{-1} in control cells to 5126 ± 1361 pg mL^{-1} and 620 ± 106 pg mL^{-1}, respectively. Treatment with Uros failed to reduce cytokine levels markedly under this condition (Fig. 2A). LPS stimulation also induced a robust elevation of IL-6 secretion, from 388 ± 86 pg mL^{-1} in control cells to 5557 ± 1290 pg mL^{-1}, and co-treatment with free Uros, including their conjugated forms, led to a significant reduction of IL-6 levels ($P < 0.05$). Notably, the free forms

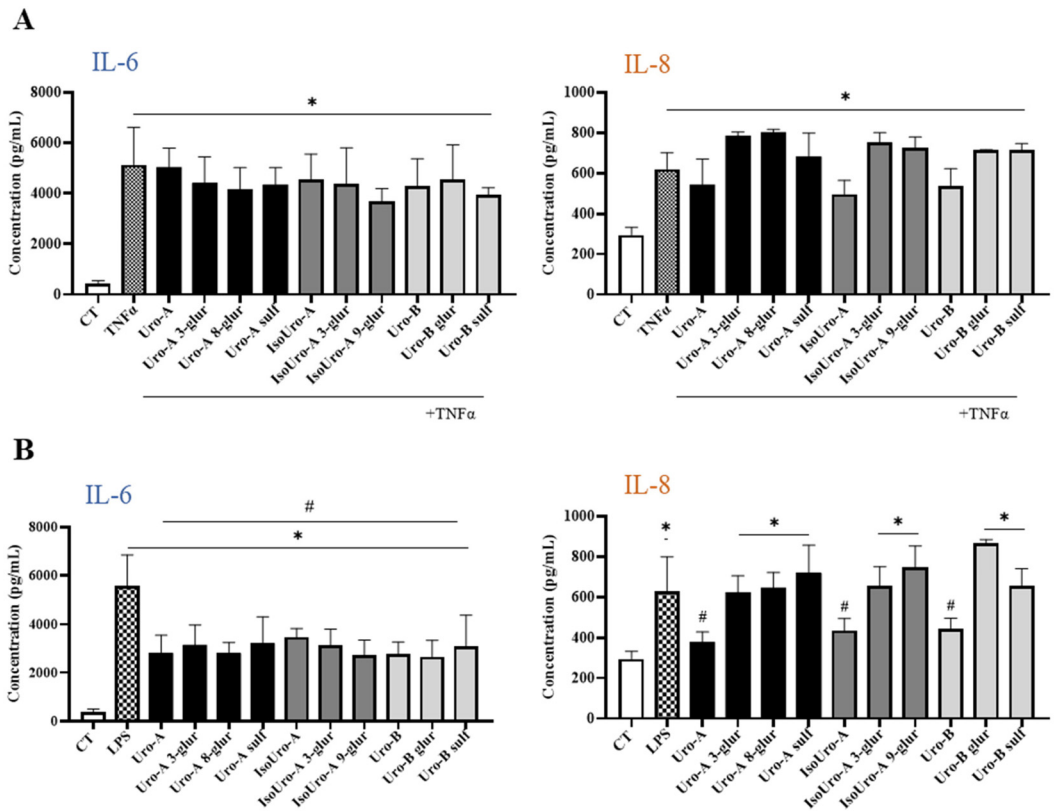

Fig. 2 Effect of urolithins (Uros) on pro-inflammatory cytokine release in HMC3 cells. (A) IL-6 and IL-8 levels in HMC3 cells stimulated with TNFα (50 ng mL^{-1}) and treated with either free urolithins or their conjugated derivatives (5 μM, 24 h). (B) IL-6 and IL-8 levels in cells stimulated with LPS (500 ng mL^{-1}) and similarly treated with urolithins. (CT; vehicle with 0.5% DMSO, non-stimulated cells). Statistical differences are denoted as $^{*}P < 0.05$ relative to CT or $^{\#}P < 0.05$ relative to TNFα or LPS. All data are presented as means ± SD ($n = 3$).

Uro-A and Uro-B decreased IL-6 concentrations to 2818 ± 733 pg mL^{-1} and 2781 ± 492 pg mL^{-1}, respectively, while the conjugates, like Uro-A 3-glur, also reduced significantly ($P < 0.05$) IL-6 levels to 3154 ± 814 pg mL^{-1} under LPS stimulation. Similarly, IL-8 induced by LPS treatment (from 289 ± 40 pg mL^{-1} to 668 ± 169 pg mL^{-1}) was also attenuated by free Uros to 379 ± 50 pg mL^{-1} (Uro-A), 419 ± 47 pg mL^{-1} (IsoUro-A), and 422 ± 47 pg mL^{-1} (Uro-B). However, this effect was not

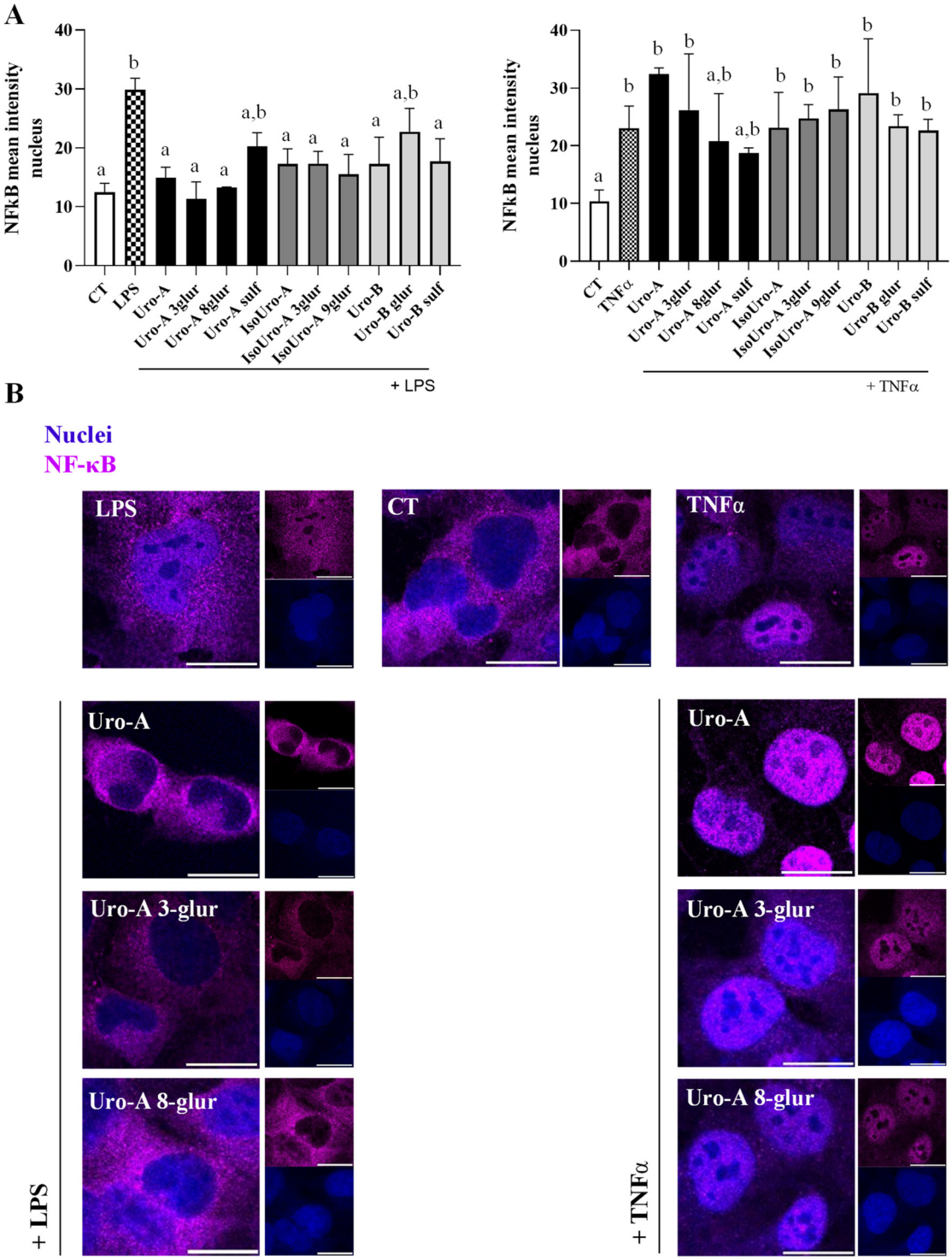

Fig. 3 Effects of Uros on NF-KB activation in HMC3 cells. (A) Quantification of NF-κB nuclear translocation in the presence of different Uros (5 μM for 45 min) following an inflammatory stimulus with LPS (500 ng mL^{-1}) or TNFα (50 ng mL^{-1}). (B) Representative immunofluorescence images show NF-κB localization (magenta) and nuclei (DAPI, blue) in selected conditions. Scale bar: 20 μm. Data are presented as mean ± SD. Different letters indicate statistically significant differences between treatments ($P < 0.05$).

observed with their conjugated counterparts (Fig. 2B). The limited efficacy of Uros under TNFα stimulation may reflect a stimulus-specific mechanism of action, possibly linked to differences in receptor signalling pathways.

Uros prevent NF-κB nuclear translocation in microglial cells

We next assessed NF-κB nuclear translocation by immunofluorescence as a marker of inflammatory activation to further explore the underlying mechanism related to the differential anti-inflammatory effects of Uros (Fig. 3 and Fig. S1). Consistent with the previous findings, the inhibitory effects of Uros were more pronounced under LPS *versus* TNFα stimulation. Semi-quantitative analysis of confocal microscopy images revealed that almost all Uros, both free and conjugated, significantly ($P < 0.05$) prevented NF-κB nuclear translocation in the presence of LPS, restoring a cytoplasmic localization pattern, in some cases comparable to control cells (Fig. 3A and Fig. S1). In contrast, only Uro-A 8-glur and Uro-A sulf showed a prevention in the NF-κB nuclear translocation in TNFα-stimulated cells. (Fig. 3 and Fig. S1). These results confirm that Uros can modulate key intracellular signalling pathways targeting the LPS-induced inflammatory route.

Table 1 Predicted binding affinities of Uros and reference compounds to the MD-2 pocket of TLR4

Molecule	Predicted binding affinity (kcal mol^{-1})
LPS	−4.5
Eritoran	−4.6
Curcumin	−7.4
Uro-A	−7.2
Uro-A 3-glur	−7.5
Uro-A 8-glur	−8.0
Uro-A sulf	−7.6
Uro-B	−7.7
Uro-B 3-glur	−8.1
Uro-B 3-sulf	−7.9
IsoUro-A	−6.8
IsoUro-A 3-glur	−8.2
IsoUro-A 9-glur	−7.8

Urolithins target the MD-2 pocket of the TLR4 receptor complex

Given that the anti-inflammatory effects of Uros were observed exclusively under LPS stimulation, we hypothesized that their mechanism of action could involve direct interaction with the TLR4/MD-2 receptor complex, which mediates LPS recognition and signalling.[36] To explore this possibility, we performed molecular docking analyses to evaluate the binding of various Uros to the MD-2 co-receptor pocket, the binding site for LPS.

The predicted binding affinities for each compound are summarized in Table 1. As expected, LPS and Eritoran, both

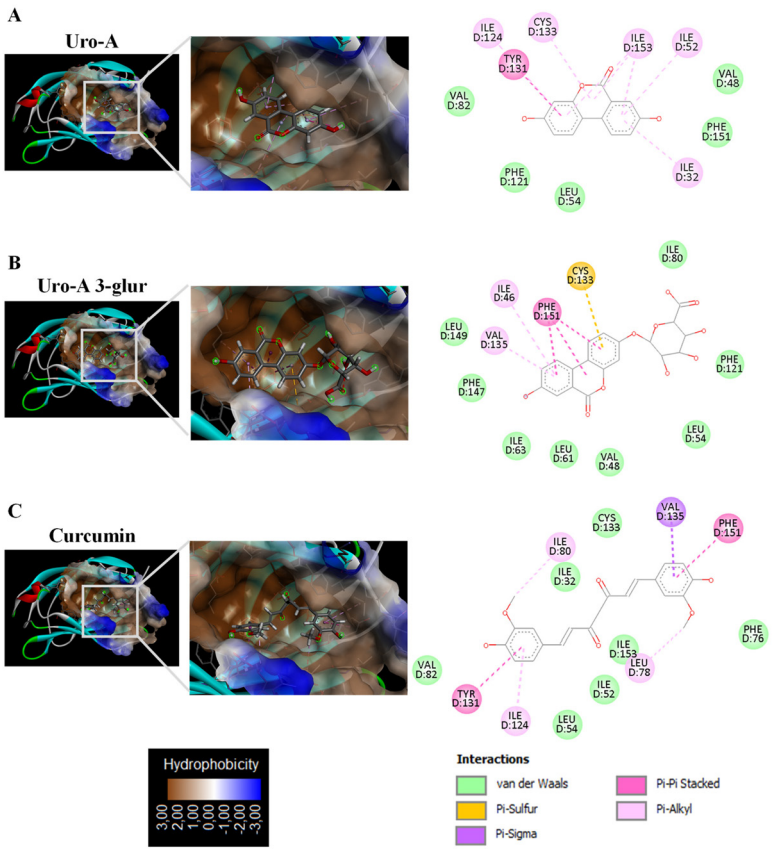

Fig. 4 Representative molecular docking poses of Uro-A (A), Uro-A 3-glur (B), and curcumin (C), within the MD-2 binding pocket of TLR4 are shown. The interactions are illustrated in 2D diagrams, highlighting key non-covalent contacts.

known ligands of the TLR4/MD-2 complex, showed relatively good binding affinities (−4.5 and −4.6 kcal mol^{-1}, respectively). Although structurally unrelated to (poly)phenols, these reference compounds were included to functionally benchmark the docking system and validate the relevance of the MD-2 binding site. In contrast, most Uros showed markedly stronger binding, with docking scores ranging from −6.8 to −8.2 kcal mol^{-1}. Notably, all Uros demonstrated robust inter-

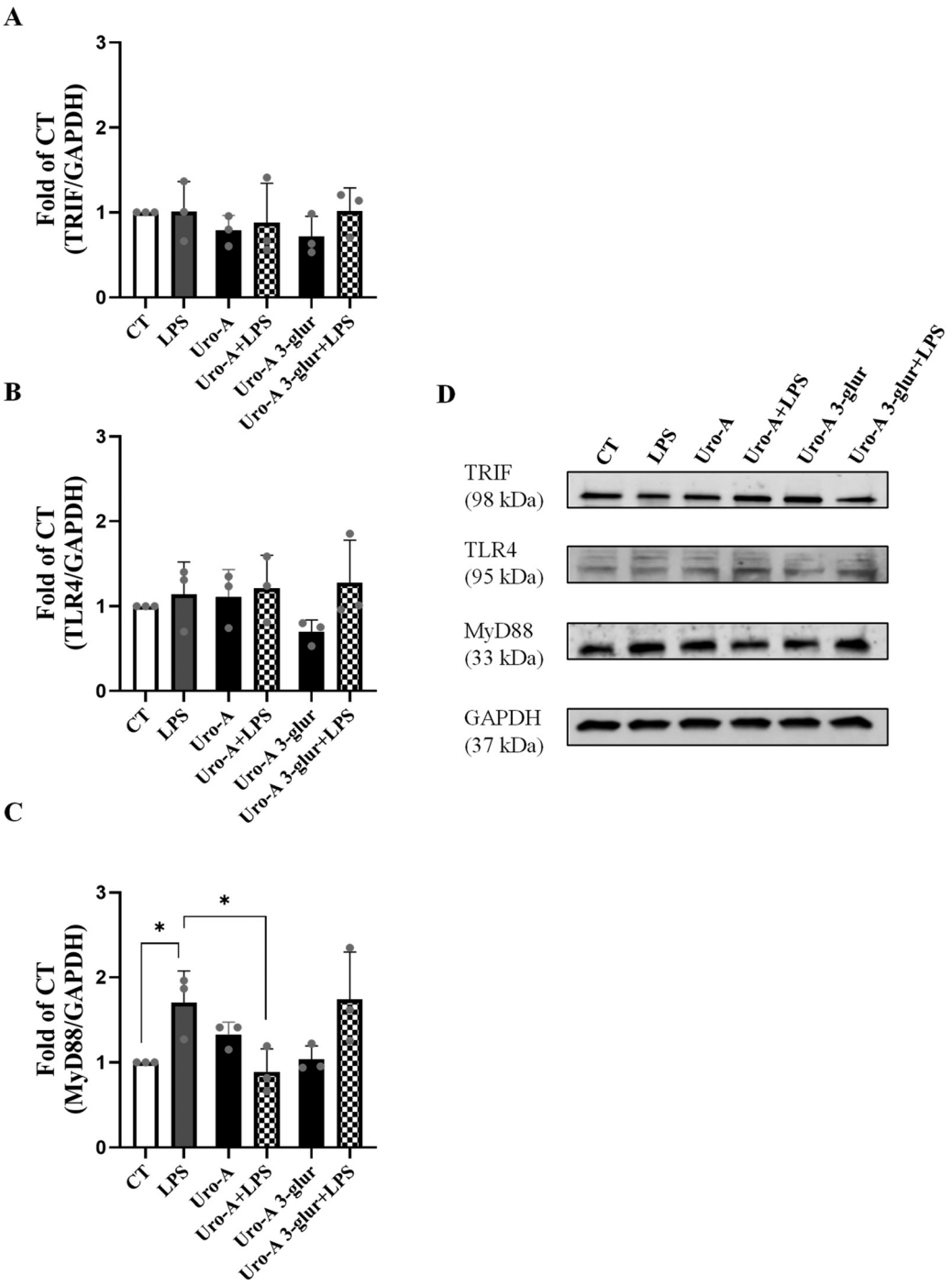

Fig. 5 Effect of Uro-A and its main circulating metabolite (Uro-A 3-glur) on the expression of TLR4 signalling proteins in LPS-stimulated HMC3 cells. Cells were stimulated with LPS (500 ng mL^{-1}) for 24 h in the absence or presence of Uros at 5 μM. The expression levels of TRIF (A), TLR4 (B), and MyD88 (C) were analysed by western blot. Representative blot images are shown in panel (D), with GAPDH used as a loading control. Data are shown as mean ± SD from three independent experiments. Data were analysed using raw values. For graphical representation, values were normalised to the mean of the control group in each experiment (control set to 1). Statistical significance was determined by the Student's *t*-test. Statistical differences are denoted as $*P < 0.05$.

actions, some of them exceeding that of curcumin (−7.4 kcal mol^{-1}), a (poly)phenol previously reported to inhibit TLR4 signalling.[37]

Uro-A and Uro-A 3-glur exhibiting values of −7.2 and −7.5 kcal mol^{-1}, respectively, close to that of curcumin (−7.4 kcal mol^{-1}). Based on the consistent biological efficacy of Uro-A showing protection in the BBB, reduction of pro-inflammatory cytokine release, and inhibition of NF-κB translocation, and the physiological relevance of Uro-A 3-glur as its major circulating metabolite in humans, these two compounds were selected for detailed interaction analysis.

The representative molecular docking poses of specific Uros and curcumin within the MD-2 binding pocket of TLR4 are shown in Fig. 4. Uro-A showed a π–π stacking interaction with Tyr131, and π–alkyl interactions with Cys133, Ile32, Ile52, Ile124, and Ile153, indicating strong hydrophobic engagement with the inner cavity of MD-2 (Fig. 4A). Uro-A 3-glur, in turn, established a π–π stacking interaction with Phe151, π–alkyl interactions with Val135 and Ile46, and a π–sulfur interaction with Cys133 (Fig. 4B). Finally, the docking analysis revealed that curcumin forms π–π stacking interactions with Tyr131 and Phe151, π–alkyl interactions with Leu78, Ile80, and Ile124, and a π–sigma interaction with Val135, stabilizing its orientation within the hydrophobic core of the MD-2 pocket (Fig. 4C).

Notably, both Uro-A and Uro-A 3-glur interact with residues critical for LPS anchoring, including Tyr131, Phe151, Val135, and Cys133, suggesting that these compounds could act as competitive inhibitors at the LPS-binding site of MD-2 and potentially suppress TLR4-driven neuroinflammatory responses.

Urolithin A downregulates MyD88 expression in LPS-stimulated microglial cells

To gain further insight into the molecular mechanisms by which Uro-A and its main circulating metabolite, Uro-A 3-glur, exert anti-inflammatory effects in microglial cells, we evaluated the expression of key proteins involved in TLR4-mediated signalling (Fig. 5). Specifically, we focused on the TLR4 receptor itself and its two major adaptor molecules, *i.e.*, MyD88, which drives the canonical NF-κB activation pathway, and TRIF, which mediates an alternative pathway leading to interferon-related responses and delayed NF-κB activation.[38,39]

Following stimulation with LPS (500 ng mL^{-1}, 24 h), we observed a significant increase ($P < 0.05$) in MyD88 protein levels, while TLR4 and TRIF expression remained unchanged compared to unstimulated control cells. This indicates that, under these conditions, LPS preferentially activates the MyD88-dependent pathway, without altering receptor abundance or TRIF-associated signalling (Fig. 5).

Co-treatment with Uro-A (5 μM) led to a selective and significant reduction ($P < 0.05$) in MyD88 protein levels, while having no appreciable effect on TLR4 or TRIF expression. In contrast, treatment with Uro-A 3-glur did not significantly affect the expression of any of the three signalling proteins analysed (Fig. 5).

Discussion

Neuroinflammation is a major contributor to neurodegenerative disease progression. Given the limited efficacy of current treatments, natural compounds like urolithins, gut microbiota-derived metabolites of dietary ETs and EA, have gained attention for their potential anti-inflammatory and neuroprotective effects.[15–17]

Nonetheless, despite increasing interest in the role of Uros in brain health, their ability to reach the brain and modulate neuroinflammatory processes remains poorly understood. In particular, it is unclear whether these metabolites, and particularly their circulating phase II conjugates, with proved lower biological properties compared that their corresponding free forms,[40,41] can effectively cross the blood–brain barrier (BBB), a critical obstacle for neurotherapeutic efficacy, and influence resident immune cells, such as microglia, which are central players in neuroinflammatory cascades.

To address these gaps, the present study investigated firstly the three major colonic Uros (Uro-A, Uro-B, and IsoUro-A) and their respective phase II conjugates' ability to cross the BBB endothelium. To this end, a simplified *in vitro* model of the human BBB was used, relying on the use of HBMECs, considered the anatomic basis of the BBB and the best human cell line for drug permeation studies, which has been previously validated, especially in BBB permeability studies.[29,32,42–45] Next, the anti-(neuro)inflammatory properties of these compounds were evaluated on both the BBB endothelium and human microglial cells (HMC3) under different inflammatory stimuli, further identifying the mechanisms of action and signalling pathways involved in this neuroprotective effect.

Transport data revealed that all Uros were able to cross the BBB in the *in vitro* model, with Uro-B and Uro-B sulf showing the highest transport efficiency, likely due to their smaller size and greater lipophilic nature. This transport has been described for other types of phenolic compounds, such as flavonoids and anthocyanins, where low molecular weight and less polar derivatives presenting methyl groups showed higher permeability through *in vitro* models of the BBB, compared to derivatives containing more polar groups.[46–48] Besides, previous transport studies using *in vitro* BBB models have also reported that other factor, such as the structural characteristics and/or position and orientation of hydroxyl groups, can modulate their transport.[49] Thus, in the case of quercetin or myrcetin, for example, intermolecular hydrogen bonds are molecular interactions that could influence their permeation through the BBB, while free hydroxyl groups may favour their transport.[50,51]

Overall, these results confirm the ability of other Uros to cross the BBB, beyond Uro-A and its sulphate conjugate, as previously reported in the perfused mouse brain.[28] Moreover, the higher transport efficiency shown by sulphate compared to glucuronide forms could explain the fact that only sulphate conjugates of Uros were detected in the brain after intraperitoneal or intravenous administration of their corresponding free Uros.[28,29] Furthermore, previous *in silico* computational

approaches predicted that free forms of Uros fulfilled criteria required for BBB penetration, but not for their sulphated and glucuronidated derivatives.[52,53] Nonetheless, other factors may contribute to explaining the observed pattern of transport specificity, beyond their physicochemical properties and affinity for the BBB. In this regard, BBB endothelial cells express tight junctions and ATP-binding cassette (ABC) transporters that prevent the brain penetration of different molecules.[54] An *in vitro* study reported that Uro-A and its sulphate conjugate, but not Uro-A glucuronides, are substrates of the human ABCG2/BCRP transporter.[55] This differential substrate specificity may help explain the lower transport efficiency of glucuronides across the BBB. Therefore, we hypothesise that the observed differences in the BBB transport of Uros and their conjugated forms could result from a combination of passive diffusion and the involvement of active transport mechanisms.

Since both free and phase II conjugated forms of Uros can cross the BBB, we assessed their potential to protect the barrier from inflammatory damage induced by TNFα. Our results demonstrated that certain Uros can effectively preserve BBB integrity, as evidenced by reductions in paracellular permeability and improvements in transendothelial electrical resistance (TEER). Specifically, Uro-A significantly decreased the permeability coefficient (*Pe*) of Na-F to near-control levels, suggesting a robust protective effect on barrier function. In parallel, TEER measurements revealed that Uro-A, IsoUro-A, and IsoUro-A 3-glur significantly attenuated the TNFα-induced decrease in electrical resistance, further supporting their role in maintaining endothelial integrity under inflammatory conditions. These findings are particularly relevant given the well-established role of BBB dysfunction in the pathogenesis of ND. Thus, disruption of the BBB is linked to increased BBB permeability, which facilitates the infiltration of neurotoxic substances and immune cells into the brain parenchyma, promoting neuroinflammation, oxidative stress, and neuronal damage.[56,57] Therefore, the ability of specific Uros to counteract inflammation-induced BBB disruption positions them as promising neuroprotective agents.

Although HBMECs constitute the first line of defence against external insults, other key triggers of neurodegeneration, such as neuroinflammation, are primarily regulated by microglia through the production of anti-inflammatory mediators and neurotrophic factors.[58] However, prolonged and excessive activation of microglia leads to the release of high levels of pro-inflammatory cytokines such as IL-6 and IL-1β, along with neurotoxic factors, which exacerbate neuroinflammation and contribute to the development of neurological disorders.[5,6,8] Consequently, reducing microglial overactivation is considered a promising therapeutic strategy for the treatment of these neurodegenerative diseases.

In this line, we next investigated the anti-(neuro)inflammatory potential of Uros and their conjugates on cytokine production in human microglial HMC3 cells, mimicking distinct inflammatory conditions, employing two well-established stimuli, *i.e.*, lipopolysaccharide (LPS), which simulates bacterial infection, and TNFα, which reflects a more physiologically relevant pro-inflammatory signal.[59,60] Our findings revealed that all tested Uros and their conjugates significantly reduced IL-6 production in LPS-stimulated HMC3 cells, indicating a potent anti-inflammatory effect under conditions of strong innate immune activation. Interestingly, only free forms of Uros significantly decreased IL-8 levels. These findings agree with previous *in vitro* studies showing that both Uro-A and Uro-B exerted strong anti-inflammatory effects in microglial murine BV2 cells by decreasing LPS-induced production of IL-6 as well as IL-1β, and TNFα, and increasing IL-10 and nitric oxide (NO).[61–66] However, the effect of phase II conjugates remained unexplored. In contrast, none of the Uros nor their conjugates produced significant effects in TNFα-treated cells, suggesting a stimulus-dependent modulation of the inflammatory response. This lack of response under TNFα stimulation, compared with the strong anti-inflammatory effect observed under LPS challenge, supports a receptor-specific, stimulus-dependent mechanism. TNFα activates the canonical NF-κB pathway through TNFR1-mediated recruitment of TRADD, TRAF2, and RIPK1, leading to IKK complex phosphorylation and nuclear translocation of NF-κB.[67] In contrast, LPS triggers both MyD88- and TRIF-dependent cascades *via* TLR4, resulting in dual activation of NF-κB and IRF3.[68] The engagement of these complementary pathways may make TLR4-driven inflammation more responsive to modulation by Uros. From a translational standpoint, this suggests that Uro-mediated protection could be particularly relevant in conditions involving endotoxin-induced neuroinflammation, such as infection-driven microglial activation, whereas TNFα-driven cytokine responses may be less sensitive to this modulation.

Notably, the involvement of NF-κB and MAPK pathways in the anti-inflammatory action of Uros was first described in IL-1β-inflamed colonic cells, where their ability to inhibit NF-κB nuclear translocation was demonstrated.[69] This foundational evidence helped establish their multi-pathway regulatory potential, now further supported by our current findings in microglial cells. Our immunochemistry analyses showed that NF-κB nuclear translocation was reduced by all Uros in LPS-stimulated HMC3 cells, with statistically significant effects for Uro-A, IsoUro-A, and Uro-B, as well as most of the conjugates. This aligns with their known modulation of key inflammatory signalling cascades, including NF-κB, Akt, and MAPK (JNK and ERK), reinforcing their broad anti-inflammatory profile under conditions of strong innate immune activation.[61,63,64] However, as expected, the inhibitory effect on NF-κB nuclear translocation was not observed under TNFα stimulation.

Furthermore, since the main target of LPS is the toll-like receptor (TLR)-4, although it is known to act on other receptors,[68] we explored whether Uros could modulate its activation in neuronal cells.[70,71] Besides, it was reported that the activation of TLR4 by LPS recruits a series of downstream adaptors, such as myeloid differentiation primary response protein 88 (MyD88) and TIR-domain-containing adaptor-inducing interferon-β (TRIF), which are crucial for the signalling of the NF-κB activation.[38,39] While our *in silico* docking analyses

suggest that both Uro-A and their conjugates can interact with residues critical for LPS anchoring within TLR4, the functional data indicate that only Uro-A selectively modulates the canonical MyD88-dependent signalling arm, without affecting the TRIF-dependent pathway. This raises the possibility that the observed suppression of NF-κB nuclear translocation and pro-inflammatory cytokine release in LPS-stimulated microglia may result from a specific interaction with the receptor that alters the recruitment or stability of adaptor proteins involved in MyD88-dependent signalling, rather than causing a complete blockade of ligand binding or TLR4 activation. Nonetheless, the *in silico* predictions require experimental validation. Binding assays would be necessary to confirm direct physical interaction with TLR4 and to map the binding sites. Such studies would help clarify whether the selectivity observed in our functional assays is due to direct receptor engagement or to indirect modulation of downstream intracellular signalling components.

Although phase II conjugates were efficiently transported across the BBB, they generally exhibited weaker biological effects than their corresponding free forms. For instance, Uro-A 3-glur showed no effect on MyD88 expression under LPS stimulation, illustrating its reduced intrinsic activity compared with Uro-A. However, it is plausible that under neuroinflammatory conditions, these conjugates could undergo enzymatic deconjugation at inflamed target tissues sites, where β-glucuronidase activity is known to be elevated.[72,73] This process may locally regenerate the active aglycones, thereby restoring biological activity *in situ*. Indeed, systemic inflammation has been shown to promote the hydrolysis of Uro-A glucuronide back to Uro-A in peripheral tissues, supporting the concept of local reactivation of conjugated metabolites under inflammatory stress.[74] Altogether, these findings reinforce the notion that Uros and their phase-II conjugates, especially Uro-A, act at multiple levels to counteract inflammation, including early modulation of intracellular signalling pathways involved in cytokine transcription.

Conclusions

Overall, our results demonstrate that circulating Uros metabolites, after the consumption of ETs and EA sources (*e.g.*, pomegranate, walnuts, or berries), can cross the BBB endothelium towards the brain, where they could exert anti-(neuro) inflammatory effects. Moreover, our findings suggest that the effects of Uros, particularly Uro-A, are more pronounced under LPS-induced acute innate immune activation and may involve downregulation of the NF-κB signalling. The lack of response to TNFα further underscores the importance of the inflammatory context in determining the efficacy of these compounds. Altogether, this study contributes to a deeper understanding of how dietary ET- and EA-rich foods may exert neuroprotective effects through the action of their microbial metabolites, potentially helping to prevent or delay neuroinflammatory processes associated with the development of ND.

Author contributions

Conceptualization: A. G-S., M. A. A-G., and J. C. E.; methodology: B. G., J. A. G-B., D. J. L-C., S. P-L.; S. N-O.; M. A. A-G., and A. G-S.; funding acquisition: A. G-S., J. A. G-B., and J. C. E.; writing original draft preparation: M. A. A-G. and A. G-S.; writing – review and editing: all authors. All authors have read and approved the final manuscript.

Conflicts of interest

There are no conflicts to declare.

Data availability

All data generated or analysed during this study are included in this published article. Supplementary information (SI): Fig. 1S: immunofluorescence images show NF-κB localization (magenta) and nuclei (DAPI, blue) in selected conditions. Scale bar: 20 μm. See DOI: https://doi.org/10.1039/d5fo03678j.

Acknowledgements

This work was supported by the grant 22030/PI/22 funded by the Programa Regional de Fomento de la Investigación Científica y Técnica (Plan de Actuación 2022) de la Fundación Séneca-Agencia de Ciencia y Tecnología de la Región de Murcia (Murcia, Spain), the Interprofessional Lemon and Grapefruit Association (AILIMPO) (Murcia, Spain), the grant CNS2022-135253 funded by MICIU/AEI/10.13039/501100011033 and by the "European Union NextGenerationEU/PRTR", the grants PID2022-136915NA-I00 and PID2022-136419OB-I00 funded by MCIN/AEI/10.13039/501100011033 and "ERDF A way of making Europe", and the AGROALNEXT program (MICIU, PRTR-C17.I1, Spain) with funding from the European Union NextGenerationEU (PRTR-C17.I1) and Fundación Séneca (Comunidad Autónoma Región de Murcia, Spain), and the grant UID 04138 funded by Instituto de Investigação do Medicamento from Portuguese Foundation for Science and Technology (FCT), Portugal. B. G-M. was funded by the grant 22777/FPI/24 (Fundación Séneca, Murcia, Spain).

References

1 Y. Hou, X. Dan, M. Babbar, Y. Wei, S. G. Hasselbalch, D. L. Croteau and V. A. Bohr, Ageing as a risk factor for neurodegenerative disease, *Nat. Rev. Neurol.*, 2019, **15**, 565–581.

2 C. Ding, Y. Wu, X. Chen, Y. Chen, Z. Wu, Z. Lin, D. Kang, W. Fang and F. Chen, Global, regional, and national burden and attributable risk factors of neurological dis-

orders: The Global Burden of Disease study 1990–2019, *Front. Public Health*, 2022, **10**, 952161.
3 M. A. DeTure and D. W. Dickson, The neuropathological diagnosis of Alzheimer's disease, *Mol. Neurodegener.*, 2019, **14**, 32.
4 G. G. Kovacs, Molecular pathology of neurodegenerative diseases: principles and practice, *J. Clin. Pathol.*, 2019, **72**, 725–735.
5 C. S. Subhramanyam, C. Wang, Q. Hu and S. T. Dheen, Microglia-mediated neuroinflammation in neurodegenerative diseases, *Semin. Cell Dev. Biol.*, 2019, **94**, 112–120.
6 W.-W. Chen, X. Zhang and W.-J. Huang, Role of neuroinflammation in neurodegenerative diseases (Review), *Mol. Med. Rep.*, 2016, **13**, 3391–3396.
7 A. S. Mendiola, J. K. Ryu, S. Bardehle, A. Meyer-Franke, K. K.-H. Ang, C. Wilson, K. M. Baeten, K. Hanspers, M. Merlini, S. Thomas, M. A. Petersen, A. Williams, R. Thomas, V. A. Rafalski, R. Meza-Acevedo, R. Tognatta, Z. Yan, S. J. Pfaff, M. R. Machado, C. Bedard, P. E. Rios Coronado, X. Jiang, J. Wang, M. A. Pleiss, A. J. Green, S. S. Zamvil, A. R. Pico, B. G. Bruneau, M. R. Arkin and K. Akassoglou, Transcriptional profiling and therapeutic targeting of oxidative stress in neuroinflammation, *Nat. Immunol.*, 2020, **21**, 513–524.
8 K. Biswas, Microglia mediated neuroinflammation in neurodegenerative diseases: A review on the cell signaling pathways involved in microglial activation, *J. Neuroimmunol.*, 2023, **383**, 578180.
9 G. Livingston, J. Huntley, A. Sommerlad, D. Ames, C. Ballard, S. Banerjee, C. Brayne, A. Burns, J. Cohen-Mansfield, C. Cooper, S. G. Costafreda, A. Dias, N. Fox, L. N. Gitlin, R. Howard, H. C. Kales, M. Kivimäki, E. B. Larson, A. Ogunniyi, V. Orgeta, K. Ritchie, K. Rockwood, E. L. Sampson, Q. Samus, L. S. Schneider, G. Selbæk, L. Teri and N. Mukadam, Dementia prevention, intervention, and care: 2020 report of the Lancet Commission, *Lancet*, 2020, **396**, 413–446.
10 M. Ayaz, F. Ullah, A. Sadiq, M. O. Kim and T. Ali, Editorial: Natural Products-Based Drugs: Potential Therapeutics Against Alzheimer's Disease and Other Neurological Disorders, *Front. Pharmacol.*, 2019, **10**, 1417.
11 E. Flanagan, D. Lamport, L. Brennan, P. Burnet, V. Calabrese, S. C. Cunnane, M. C. de Wilde, L. Dye, J. A. Farrimond, N. Emerson Lombardo, T. Hartmann, T. Hartung, M. Kalliomäki, G. G. Kuhnle, G. La Fata, A. Sala-Vila, C. Samieri, A. D. Smith, J. P. E. Spencer, S. Thuret, K. Tuohy, S. Turroni, W. Vanden Berghe, M. Verkuijl, K. Verzijden, M. Yannakoulia, L. Geurts and D. Vauzour, Nutrition and the ageing brain: Moving towards clinical applications, *Ageing Res. Rev.*, 2020, **62**, 101079.
12 R. González-Domínguez, P. Castellano-Escuder, F. Carmona, S. Lefèvre-Arbogast, D. Y. Low, A. Du Preez, S. R. Ruigrok, C. Manach, M. Urpi-Sarda, A. Korosi, P. J. Lucassen, L. Aigner, M. Pallàs, S. Thuret, C. Samieri, A. Sánchez-Pla and C. Andres-Lacueva, Food and Microbiota Metabolites Associate with Cognitive Decline in Older Subjects: A 12-Year Prospective Study, *Mol. Nutr. Food Res.*, 2021, **65**, 2100606.
13 S. N. A. Bukhari, Dietary Polyphenols as Therapeutic Intervention for Alzheimer's Disease: A Mechanistic Insight, *Antioxidants*, 2022, **11**, 554.
14 A. González-Sarrías, F. A. Tomás-Barberán and R. García-Villalba, in *Dietary Polyphenols*, John Wiley & Sons, Ltd, 2020, pp. 1–29.
15 R. García-Villalba, F. A. Tomás-Barberán, C. E. Iglesias-Aguirre, J. A. Giménez-Bastida, A. González-Sarrías, M. V. Selma and J. C. Espín, Ellagitannins, urolithins, and neuroprotection: Human evidence and the possible link to the gut microbiota, *Mol. Aspects Med.*, 2023, **89**, 101109.
16 F. A. Tomás-Barberán, A. González-Sarrías, R. García-Villalba, M. A. Núñez-Sánchez, M. V. Selma, M. T. García-Conesa and J. C. Espín, Urolithins, the rescue of "old" metabolites to understand a "new" concept: Metabotypes as a nexus among phenolic metabolism, microbiota dysbiosis, and host health status, *Mol. Nutr. Food Res.*, 2017, **61**, 1500901.
17 R. García-Villalba, J. A. Giménez-Bastida, A. Cortés-Martín, M. Á. Ávila-Gálvez, F. A. Tomás-Barberán, M. V. Selma, J. C. Espín and A. González-Sarrías, Urolithins: a Comprehensive Update on their Metabolism, Bioactivity, and Associated Gut Microbiota, *Mol. Nutr. Food Res.*, 2022, **66**, 2101019.
18 F. A. Tomás-Barberán, R. García-Villalba, A. González-Sarrías, M. V. Selma and J. C. Espín, Ellagic Acid Metabolism by Human Gut Microbiota: Consistent Observation of Three Urolithin Phenotypes in Intervention Trials, Independent of Food Source, Age, and Health Status, *J. Agric. Food Chem.*, 2014, **62**, 6535–6538.
19 A. Cortés-Martín, M. V. Selma, F. A. Tomás-Barberán, A. González-Sarrías and J. C. Espín, Where to Look into the Puzzle of Polyphenols and Health? The Postbiotics and Gut Microbiota Associated with Human Metabotypes, *Mol. Nutr. Food Res.*, 2020, **64**, 1900952.
20 D. D'Amico, P. A. Andreux, P. Valdés, A. Singh, C. Rinsch and J. Auwerx, Impact of the Natural Compound Urolithin A on Health, Disease, and Aging, *Trends Mol. Med.*, 2021, **27**, 687–699.
21 O. Wojciechowska and M. Kujawska, Urolithin A in Health and Diseases: Prospects for Parkinson's Disease Management, *Antioxidants*, 2023, **12**, 1479.
22 L. An, Q. Lu, K. Wang and Y. Wang, Urolithins: A Prospective Alternative against Brain Aging, *Nutrients*, 2023, **15**, 3884.
23 G. R. Gandhi, P. J. Antony, S. A. Ceasar, A. B. S. Vasconcelos, M. M. Montalvão, M. N. Farias de Franca, A. d. S. Resende, C. S. Sharanya, Y. Liu, G. Hariharan and R.-Y. Gan, Health functions and related molecular mechanisms of ellagitannin-derived urolithins, *Crit. Rev. Food Sci. Nutr.*, 2024, **64**, 280–310.
24 A. González-Sarrías, M. Á. Núñez-Sánchez, F. A. Tomás-Barberán and J. C. Espín, Neuroprotective Effects of

Bioavailable Polyphenol-Derived Metabolites against Oxidative Stress-Induced Cytotoxicity in Human Neuroblastoma SH-SY5Y Cells, *J. Agric. Food Chem.*, 2017, **65**, 752–758.

25 M. Gasperotti, S. Passamonti, F. Tramer, D. Masuero, G. Guella, F. Mattivi and U. Vrhovsek, Fate of Microbial Metabolites of Dietary Polyphenols in Rats: Is the Brain Their Target Destination?, *ACS Chem. Neurosci.*, 2015, **6**, 1341–1352.

26 M. Kujawska, M. Jourdes, Ł. Witucki, M. Karaźniewicz-Łada, M. Szulc, A. Górska, P. Ł. Mikołajczak, P.-L. Teissedre and J. Jodynis-Liebert, Pomegranate Juice Ameliorates Dopamine Release and Behavioral Deficits in a Rat Model of Parkinson's Disease, *Brain Sci.*, 2021, **11**, 1127.

27 M. Kujawska, M. Jourdes, M. Kurpik, M. Szulc, H. Szaefer, P. Chmielarz, G. Kreiner, V. Krajka-Kuźniak, P. Ł. Mikołajczak, P.-L. Teissedre and J. Jodynis-Liebert, Neuroprotective Effects of Pomegranate Juice against Parkinson's Disease and Presence of Ellagitannins-Derived Metabolite—Urolithin A—In the Brain, *Int. J. Mol. Sci.*, 2020, **21**, 202.

28 J. I. Jiménez-Loygorri, B. Villarejo-Zori, Á. Viedma-Poyatos, J. Zapata-Muñoz, R. Benítez-Fernández, M. D. Frutos-Lisón, F. A. Tomás-Barberán, J. C. Espín, E. Area-Gómez, A. Gomez-Duran and P. Boya, Mitophagy curtails cytosolic mtDNA-dependent activation of cGAS/STING inflammation during aging, *Nat. Commun.*, 2024, **15**(1), 830.

29 M. Á. Ávila-Gálvez, B. Garay-Mayol, A. Marín, M. A. Brito, J. A. Giménez-Bastida, J. C. Espín and A. González-Sarrías, Metabolic Profiling of a Mediterranean-Inspired (Poly) phenol-Rich Mixture in the Brain: Perfusion Effect and In Vitro Blood–Brain Barrier Transport Validation, *J. Agric. Food Chem.*, 2025, **73**, 11056–11066.

30 M. F. Stins, J. Badger and K. Sik Kim, Bacterial invasion and transcytosis in transfected human brain microvascular endothelial cells, *Microb. Pathog.*, 2001, **30**, 19–28.

31 I. Figueira, G. Garcia, R. C. Pimpão, A. P. Terrasso, I. Costa, A. F. Almeida, L. Tavares, T. F. Pais, P. Pinto, M. R. Ventura, A. Filipe, G. J. McDougall, D. Stewart, K. S. Kim, I. Palmela, D. Brites, M. A. Brito, C. Brito and C. N. Santos, Polyphenols journey through blood-brain barrier towards neuronal protection, *Sci. Rep.*, 2017, **7**, 11456.

32 M. Á. Ávila-Gálvez, B. Garay-Mayol, J. A. Giménez-Bastida, M. d. C. L. de las Hazas, C. Mazarío-Gárgoles, M. A. Brito, A. Dávalos, J. C. Espín and A. González-Sarrías, Enhanced brain delivery and antiproliferative activity of resveratrol using milk-derived exosomes, *J. Agric. Food Res.*, 2024, **18**, 101370.

33 M. A. Deli, C. S. Ábrahám, Y. Kataoka and M. Niwa, Permeability Studies on In Vitro Blood–Brain Barrier Models:Physiology, Pathology, and Pharmacology, *Cell. Mol. Neurobiol.*, 2005, **25**, 59–127.

34 J. A. Giménez-Bastida, M. Á. Ávila-Gálvez, J. C. Espín and A. González-Sarrías, Conjugated Physiological Resveratrol Metabolites Induce Senescence in Breast Cancer Cells: Role of p53/p21 and p16/Rb Pathways, and ABC Transporters, *Mol. Nutr. Food Res.*, 2019, **63**, 1900629.

35 M. Á. Ávila-Gálvez, R. García-Villalba, F. Martínez-Díaz, B. Ocaña-Castillo, T. Monedero-Saiz, A. Torrecillas-Sánchez, B. Abellán, A. González-Sarrías and J. C. Espín, Metabolic Profiling of Dietary Polyphenols and Methylxanthines in Normal and Malignant Mammary Tissues from Breast Cancer Patients, *Mol. Nutr. Food Res.*, 2019, **63**, 1801239.

36 H. M. Kim, B. S. Park, J.-I. Kim, S. E. Kim, J. Lee, S. C. Oh, P. Enkhbayar, N. Matsushima, H. Lee, O. J. Yoo and J.-O. Lee, Crystal Structure of the TLR4-MD-2 Complex with Bound Endotoxin Antagonist Eritoran, *Cell*, 2007, **130**, 906–917.

37 H. Gradišar, M. M. Keber, P. Pristovšek and R. Jerala, MD-2 as the target of curcumin in the inhibition of response to LPS, *J. Leukocyte Biol.*, 2007, **82**, 968–974.

38 A. Płóciennikowska, A. Hromada-Judycka, K. Borzęcka and K. Kwiatkowska, Co-operation of TLR4 and raft proteins in LPS-induced pro-inflammatory signaling, *Cell. Mol. Life Sci.*, 2015, **72**, 557–581.

39 P. Zhang, M. Yang, C. Chen, L. Liu, X. Wei and S. Zeng, Toll-Like Receptor 4 (TLR4)/Opioid Receptor Pathway Crosstalk and Impact on Opioid Analgesia, Immune Function, and Gastrointestinal Motility, *Front. Immunol.*, 2020, **11**, 1455.

40 A. González-Sarrías, J. A. Giménez-Bastida, M. Á. Núñez-Sánchez, M. Larrosa, M. T. García-Conesa, F. A. Tomás-Barberán and J. C. Espín, Phase-II metabolism limits the antiproliferative activity of urolithins in human colon cancer cells, *Eur. J. Nutr.*, 2014, **53**, 853–864.

41 M. Á. Ávila-Gálvez, J. C. Espín and A. González-Sarrías, Physiological Relevance of the Antiproliferative and Estrogenic Effects of Dietary Polyphenol Aglycones versus Their Phase-II Metabolites on Breast Cancer Cells: A Call of Caution, *J. Agric. Food Chem.*, 2018, **66**, 8547–8555.

42 D. E. Eigenmann, G. Xue, K. S. Kim, A. V. Moses, M. Hamburger and M. Oufir, Comparative study of four immortalized human brain capillary endothelial cell lines, hCMEC/D3, hBMEC, TY10, and BB19, and optimization of culture conditions, for an in vitro blood–brain barrier model for drug permeability studies, *Fluids Barriers CNS*, 2013, **10**, 33.

43 D. E. Eigenmann, E. A. Jähne, M. Smieško, M. Hamburger and M. Oufir, Validation of an immortalized human (hBMEC) in vitro blood-brain barrier model, *Anal. Bioanal. Chem.*, 2016, **408**, 2095–2107.

44 I. Palmela, F. L. Cardoso, M. Bernas, L. Correia, A. R. Vaz, R. F. M. Silva, A. Fernandes, K. S. Kim, D. Brites and M. A. Brito, Elevated Levels of Bilirubin and Long-Term Exposure Impair Human Brain Microvascular Endothelial Cell Integrity, *Curr. Neurovasc. Res.*, 2011, **8**, 153–169.

45 I. Palmela, L. Correia, R. F. M. Silva, H. Sasaki, K. S. Kim, D. Brites and M. A. Brito, Hydrophilic bile acids protect human blood-brain barrier endothelial cells from disruption by unconjugated bilirubin: an in vitro study, *Front. Neurosci.*, 2015, **9**, 80.

46 K. A. Youdim, M. S. Dobbie, G. Kuhnle, A. R. Proteggente, N. J. Abbott and C. Rice-Evans, Interaction between flavonoids and the blood–brain barrier: in vitro studies, *J. Neurochem.*, 2003, **85**, 180–192.

47 K. A. Youdim, M. Z. Qaiser, D. J. Begley, C. A. Rice-Evans and N. J. Abbott, Flavonoid permeability across an in situ model of the blood–brain barrier, *Free Radicals Biol. Med.*, 2004, **36**, 592–604.

48 A. Faria, M. Meireles, I. Fernandes, C. Santos-Buelga, S. Gonzalez-Manzano, M. Dueñas, V. de Freitas, N. Mateus and C. Calhau, Flavonoid metabolites transport across a human BBB model, *Food Chem.*, 2014, **149**, 190–196.

49 A. Faria, D. Pestana, D. Teixeira, P.-O. Couraud, I. Romero, B. Weksler, V. de Freitas, N. Mateus and C. Calhau, Insights into the putative catechin and epicatechin transport across blood-brain barrier, *Food Funct.*, 2011, **2**, 39–44.

50 C. Chen, J. Zhou and C. Ji, Quercetin: A potential drug to reverse multidrug resistance, *Life Sci.*, 2010, **87**, 333–338.

51 I. Figueira, L. Tavares, C. Jardim, I. Costa, A. P. Terrasso, A. F. Almeida, C. Govers, J. J. Mes, R. Gardner, J. D. Becker, G. J. McDougall, D. Stewart, A. Filipe, K. S. Kim, D. Brites, C. Brito, M. A. Brito and C. N. Santos, Blood–brain barrier transport and neuroprotective potential of blackberry-digested polyphenols: an in vitro study, *Eur. J. Nutr.*, 2019, **58**, 113–130.

52 T. Yuan, H. Ma, W. Liu, D. B. Niesen, N. Shah, R. Crews, K. N. Rose, D. A. Vattem and N. P. Seeram, Pomegranate's Neuroprotective Effects against Alzheimer's Disease Are Mediated by Urolithins, Its Ellagitannin-Gut Microbial Derived Metabolites, *ACS Chem. Neurosci.*, 2016, **7**, 26–33.

53 G. Aichinger, M. Stevanoska, K. Beekmann and S. J. Sturla, Physiologically-Based Pharmacokinetic Modeling of the Postbiotic Supplement Urolithin A Predicts its Bioavailability Is Orders of Magnitude Lower than Concentrations that Induce Toxicity, but also Neuroprotective Effects, *Mol. Nutr. Food Res.*, 2023, **67**, 2300009.

54 Y. He, Y. Yao, S. E. Tsirka and Y. Cao, Cell-Culture Models of the Blood–Brain Barrier, *Stroke*, 2014, **45**, 2514–2526.

55 A. González-Sarrías, V. Miguel, G. Merino, R. Lucas, J. C. Morales, F. Tomás-Barberán, A. I. Álvarez and J. C. Espín, The Gut Microbiota Ellagic Acid-Derived Metabolite Urolithin A and Its Sulfate Conjugate Are Substrates for the Drug Efflux Transporter Breast Cancer Resistance Protein (ABCG2/BCRP), *J. Agric. Food Chem.*, 2013, **61**, 4352–4359.

56 B. T. Hawkins and T. P. Davis, The Blood-Brain Barrier/Neurovascular Unit in Health and Disease, *Pharmacol. Rev.*, 2005, **57**, 173–185.

57 S. Chen, L. Shao and L. Ma, Cerebral Edema Formation After Stroke: Emphasis on Blood–Brain Barrier and the Lymphatic Drainage System of the Brain, *Front. Cell. Neurosci.*, 2021, **15**, 716825.

58 K. Haruwaka, A. Ikegami, Y. Tachibana, N. Ohno, H. Konishi, A. Hashimoto, M. Matsumoto, D. Kato, R. Ono, H. Kiyama, A. J. Moorhouse, J. Nabekura and H. Wake, Dual microglia effects on blood brain barrier permeability induced by systemic inflammation, *Nat. Commun.*, 2019, **10**, 5816.

59 V. H. Perry, The influence of systemic inflammation on inflammation in the brain: implications for chronic neurodegenerative disease, *Brain, Behav., Immun.*, 2004, **18**, 407–413.

60 K. M. Lucin and T. Wyss-Coray, Immune activation in brain aging and neurodegeneration: too much or too little?, *Neuron*, 2009, **64**, 110–122.

61 J. Xu, C. Yuan, G. Wang, J. Luo, H. Ma, L. Xu, Y. Mu, Y. Li, N. P. Seeram, X. Huang and L. Li, Urolithins Attenuate LPS-Induced Neuroinflammation in BV2Microglia via MAPK, Akt, and NF-κB Signaling Pathways, *J. Agric. Food Chem.*, 2018, **66**, 571–580.

62 N. A. DaSilva, P. P. Nahar, H. Ma, A. Eid, Z. Wei, S. Meschwitz, N. H. Zawia, A. L. Slitt and N. P. Seeram, Pomegranate ellagitannin-gut microbial-derived metabolites, urolithins, inhibit neuroinflammation in vitro, *Nutr. Neurosci.*, 2019, **22**, 185–195.

63 R. Velagapudi, I. Lepiarz, A. El-Bakoush, F. O. Katola, H. Bhatia, B. L. Fiebich and O. A. Olajide, Induction of Autophagy and Activation of SIRT-1 Deacetylation Mechanisms Mediate Neuroprotection by the Pomegranate Metabolite Urolithin A in BV2 Microglia and Differentiated 3D Human Neural Progenitor Cells, *Mol. Nutr. Food Res.*, 2019, **63**, 1801237.

64 G. Lee, J.-S. Park, E.-J. Lee, J.-H. Ahn and H.-S. Kim, Anti-inflammatory and antioxidant mechanisms of urolithin B in activated microglia, *Phytomedicine*, 2019, **55**, 50–57.

65 A. M. Toney, M. Albusharif, D. Works, L. Polenz, S. Schlange, V. Chaidez, A. E. Ramer-Tait and S. Chung, Differential Effects of Whole Red Raspberry Polyphenols and Their Gut Metabolite Urolithin A on Neuroinflammation in BV-2 Microglia, *Int. J. Environ. Res. Public Health*, 2021, **18**, 68.

66 J. Qiu, Y. Chen, J. Zhuo, L. Zhang, J. Liu, B. Wang, D. Sun, S. Yu and H. Lou, Urolithin A promotes mitophagy and suppresses NLRP3 inflammasome activation in lipopolysaccharide-induced BV2 microglial cells and MPTP-induced Parkinson's disease model, *Neuropharmacology*, 2022, **207**, 108963.

67 H. Li and X. Lin, Positive and negative signaling components involved in TNFα-induced NF-κB activation, *Cytokine*, 2008, **41**, 1–8.

68 C. R. A. Batista, G. F. Gomes, E. Candelario-Jalil, B. L. Fiebich and A. C. P. de Oliveira, Lipopolysaccharide-Induced Neuroinflammation as a Bridge to Understand Neurodegeneration, *Int. J. Mol. Sci.*, 2019, **20**, 2293.

69 A. González-Sarrías, M. Larrosa, F. A. Tomás-Barberán, P. Dolara and J. C. Espín, NF-κB-dependent anti-inflammatory activity of urolithins, gut microbiota ellagic acid-derived metabolites, in human colonic fibroblasts, *Br. J. Nutr.*, 2010, **104**, 503–512.

70 A. Rolls, R. Shechter, A. London, Y. Ziv, A. Ronen, R. Levy and M. Schwartz, Toll-like receptors modulate adult

hippocampal neurogenesis, *Nat. Cell Biol.*, 2007, **9**, 1081–1088.

71 S. Leow-Dyke, C. Allen, A. Denes, O. Nilsson, S. Maysami, A. G. Bowie, N. J. Rothwell and E. Pinteaux, Neuronal toll-like receptor 4 signaling induces brain endothelial activation and neutrophil transmigration in vitro, *J. Neuroinflammation*, 2012, **9**, 230.

72 K. Shimoi and T. Nakayama, in *Methods in Enzymology*, Academic Press, 2005, vol. 400, pp. 263–272.

73 A. A. Allam, H. A. Rudayni, N. A. Ahmed, F. F. A. Alkhayl, A. M. Lamsabhi and E. M. Kamel, β-Glucuronidase Inhibition in Drug Development: Emerging Strategies for Mitigating Drug-Induced Toxicity and Enhancing Therapeutic Outcomes, *Drug Dev. Res.*, 2025, **86**, e70118.

74 M. A. Ávila-Gálvez, J. A. Giménez-Bastida, A. González-Sarrías and J. C. Espín, Tissue deconjugation of urolithin A glucuronide to free urolithin A in systemic inflammation, *Food Funct.*, 2019, **10**, 3135–3141.